Issue VI, 22 November 2023
e-ISSN 2707-9481 Institute of Metallurgy and Ore Beneficiation, Satbayev University, Almaty, Kazakhstan
ISBN 978-601-323-356-7 https://doi.org/10.31643/2023.13

Maksim A. Pakhomov
Kutateladze Institute of Thermophysics, Siberian Branch of the Russian Academy of Science, Lavrent'ev Ave., 1, 630090, Novosibirsk, Russia
E-mail: pakhomov@itp.nsc.ru

Uzak K. Zhapbasbayev
Satbayev University, 050013, Satpaev str, 22a, Almaty, Kazakhstan
https://orcid.org/0000-0001-5973-5149
E-mail: uzak.zh@mail.ru

RANS modeling of the transition of a non-isothermal flow of a Newtonian fluid to a viscoplastic state in a pipe

Abstract: A mathematical model of the movement and heat transfer of a turbulent non-isothermal non-Newtonian fluid through a pipe wall with a cold surrounding space has been developed and simulated numerically. Fluid turbulence is described in the framework of the isotropic two-parameter k–$\tilde{\varepsilon}$ model. The Newtonian properties of the fluid in the initial cross-sections of the pipe transformed gradually into a viscoplastic non-Newtonian Bingham-Schwedoff fluid state due to heat transfer through the pipe wall between the heated fluid and a cold environment. The value of its streamwise velocity in the axial zone increased significantly when the fluid moved along the pipe. On the contrary, it decreased in the near-wall zone and the height of the region with a zero fluid velocity increased. This occurred due to the viscoplastic properties of a non-Newtonian fluid. The height of the region with a zero fluid velocity in the pipe increased gradually as the non-Newtonian fluid (waxy crude oil) moved through the pipe. A noticeable increase in the level of turbulent kinetic energy in the axial zone of the pipe and its noticeable decrease in its near-wall region were observed. A significant increase in the average dynamic viscosity and yield stress in the near-wall part of the pipe was shown. The boundary of the area of existence of Newtonian properties of fluid was determined. The height of the region with a zero fluid velocity in the pipe increased gradually as waxy crude oil moved through the pipe and reached $y/R \approx 0.1$ at $x/D = 15$.

Keywords: RANS, Newtonian and non-Newtonian fluids, Bingham-Schwedoff fluid, viscoplastic, yield stress, turbulent flow, heat transfer.

Cite this article as: Pakhomov M.A., Zhapbasbayev U.K. RANS modeling of the transition of a non-isothermal flow of a Newtonian fluid to a viscoplastic state in a pipe. *Challenges of Science*. Issue VI, 2023, pp. 108-123. https://doi.org/10.31643/2023.13

Introduction

Turbulent non-isothermal flows of non-Newtonian viscoplastic fluids in pipes (Bingham-Schwedoff fluid) are of great practical importance (Barnes, 1999), since they are found in many industrial installations (various heat exchangers, pipelines, bearings, centrifuges, oil production from deep water, wastewater treatment systems, etc.). One example of such a fluid is waxy crude oil. Considering the latest discoveries in geological exploration, the value of such oil reserves will only increase in the future. The main difficulties associated with transporting such a fluid through pipelines are the strong dependence of viscosity and yield shear stress on fluid temperatures due to their content of asphaltenes, paraffins, and resins (see monographs by Beisembetov et al., 2016; Tugunov & Novoselov, 1972) and reviews (Aiyejina et al., 2011; Chala et al., 2018; Elkatory et al., 2022). Waxy crude oil at high temperatures obeys the laws of a Newtonian fluid, and when its temperature decreases, the viscoplastic properties of non-Newtonian fluids appear (Aiyejina et al., 2011; Chala et al., 2018; Elkatory et al., 2022). Such oils have a high solidification point (from 285–303 K), which can be higher than the temperature of the surrounding soil environment (Beisembetov et al., 2016; Zhao et al., 2020; Ghannam et al., 2012). The flow of waxy oil, which is originally a Newtonian fluid, is cooled by heat transfer into a colder environment through the pipe wall. This leads to a change in the rheological and physicochemical properties of the oil along the pipe length. The complex rheological properties of such fluids are characterized by a sharp increase in viscosity at a decrease in their temperature (Beisembetov et al., 2016; Zhao et al., 2020).

Finally, it causes appearance of a critical stress value, it is also known as the yield stress (Barnes, 1999; Beisembetov et al., 2016).

One of the rheological properties of waxy oil is its yield shear stress, which can cause the formation of a "stagnant zone", where the flow velocity is zero (Chala et al., 2018; Beisembetov et al., 2016). This also leads to a decrease in the working area of the pipe cross-section (Chala et al., 2018). The formation of a "stagnant zone" can lead to two scenarios for the development of the flow of a complex rheological fluid. In the case of insufficient kinetic and thermal energy of the flow, the "stagnant zone" blocks the working cross-section of the pipeline, the hydraulic resistance increases sharply, and the pipeline section becomes "frozen" (Ghannam et al., 2012; Zhao, 2020; Zhapbasbayev et al., 2021; Hussain et al., 2023). If the kinetic and thermal energy of the fluid flow is sufficient, then with a decrease in the working cross-section of the pipe, the flow velocity increases, and this leads to the dissipation of the kinetic energy of the flow to the thermal energy near the "stagnant zone" boundary (Beisembetov et al., 2016). The velocity magnitude increases from the wall to the pipe center in this case and the velocity gradient in the region of the boundary between the "stagnant zone" and the flow of the Newtonian fluid also increases. This leads to the self-heating of the fluid in this area (the amount of heat generated is directly proportional to the square of the velocity gradient (Beisembetov et al., 2016). Within the theoretical limits, the flow enters the regime of a "hydrodynamic thermal explosion" (Bostanjiyan & Chernyaeva, 1966). Heat losses along the pipe length decrease due to an increase in the flow velocity and the fact that the fluid near the pipe walls serves as a thermal insulator. The area of the "stagnant zone" stabilizes in practice (Aiyejina et al., 2011), and the friction along the pipe length decreases (Beisembetov et al., 2016; Tugunov & Novoselov et al., 1972).

The complex rheological properties of a Bingham-Schwedoff (BS) fluid are determined by a nonlinear increase in viscosity and yield shear stress with a decrease in its temperature, which leads to the non-Newtonian state of a waxy crude oil. For laminar flow regimes, many publications have focused on the study of heat transfer in such fluids flowing in a pipe (Zhao, 2020; Bostanjiyan & Chernyaeva, 1966) and behind a backward-facing step (Danane et al., 2020). Some works have dealt with the study of the turbulent flow of a non-Newtonian polymer solution (viscoelastic) (Cruz & Pinho, 2003; Iaccarino et al., 2010; Masoudian et al., 2016), power law (Gavrilov & Rudyak, 2016), Herschel–Bulkley (Malin, 1997) and BS (Pakhomov & Zhapbasbayev, 2021) fluids. These studies used various models of turbulence at different levels: k–ε (Cruz & Pinho, 2003; Iaccarino et al., 2010; Malin, 1997; Pakhomov & Zhapbasbayev, 2021), $v2$–f (Masoudian et al., 2016; Gavrilov & Rudyak, 2016) and k–ω SST (Lovato, et al., 2022). The complexity of the numerical modeling of such flows connected to the developed turbulence models can hardly be verified directly using the experimental benchmark. It should be noted that the level of turbulence anisotropy of a non-Newtonian fluid is higher than that of a Newtonian fluid (Masoudian et al., 2016; Sahu et al., 2007). A few large eddy simulation (LES) (Gnambode et al., 2015; Amani et al., 2023) and direct numerical simulation (DNS) (Gavrilov & Rudyak, 2017; Singh et al., 2017) studies have been carried out to study visco- and pseudo-plastic turbulent fluids in the last two decades. Data were obtained on the mean streamwise velocity, distributions of the components of the Reynolds stress tensor, wall friction, balance of shear stresses, and the turbulent kinetic energy for a steady turbulent flow with Reynolds numbers in the range Re = 5000–20000. Heat transfer in such flows has not yet been considered in the literature, and only one recent work has been found (Gnambode et al., 2015). The DNS and Reynolds-averaged Navier–Stokes (RANS) studies of fluid flow and heat transfer for a non-Newtonian turbulent liquid polymer were carried out in this paper. The time mean statistics of temperature fluctuations, turbulent heat flux, thermal turbulent diffusivity, and budget in terms of the temperature variance were predicted and compared with those of the Newtonian fluid.

The study of mixing and linear instability of miscible and immiscible Newtonian and non-Newtonian fluids has great importance due to the relevance in chemical industry and waxy crude oil transportation through the pipelines (Usha & Sahu, 2019).

It should be noted that the results of numerical studies of the flow turbulent structure and heat transfer in the process of transition of the Newtonian turbulent BS fluid (waxy crude oil) in pipes to the non-Newtonian viscoplastic fluid has not yet been presented in the literature, except our recent paper (Pakhomov & Zhapbasbayev, 2021). The aim of the present paper is to investigate the flow and heat transfer in a turbulent hydrodynamically steady-state incompressible non-Newtonian fluid flowing through a pipe. This study may be of interest to scientists and research engineers dealing with the design and transport of waxy crude oils in pipelines. This present book chapter is an extended form of previously published article in the following journal Case Studies Thermal Engineering (Pakhomov & Zhapbasbayev, 2021).

Mathematical model

Physical Model of a Non-Newtonian Viscoplastic (Bingham-Schwedoff) Fluid

A schematic view of the flow configuration is shown in Fig. 1. A non-isothermal viscoplastic non-Newtonian fluid (waxy crude oil) flow along an underground pipe with an inner diameter (I.D.) $D = 2R = 0.2$ m, length $L = 3$ m, and depth to pipe axis $H = 2$ m. The mean-mass velocity of the liquid flow at the pipe inlet was $U_{m1} = 0.2$ m/s and its initial temperature $T_1 = 298$ K. The ambient temperature (soil) was $T_{Soil} = 273–298$ K. The pipe material was stainless steel and the pipe wall thickness $\delta = 2$ mm. It was assumed that the temperature of the pipe wall from its outer side was equal to the soil temperature $T_{W2} = T_{Soil}$. The temperature of soil was a constant value. The density of fluid flow in the inlet cross-section $\rho_1 = 835$ kg/m^3. The Reynolds number of the flow, determined from the flow parameters at the inlet (for a Newtonian fluid) $\mathrm{Re} = U_{m1}D_1/\nu_{W1} = 8200$.

A few problems regarding the development of a mathematical model of any non-Newtonian turbulent fluid based on Reynolds-averaged equations (RANS) have to be solved (Gavrilov & Rudyak, 2016): 1) a model for the averaged effective dynamics viscosity coefficient should be developed; 2) a closure for correlations of the viscosity pulsation with the strain rate tensor, which does not appear for a Newtonian turbulent fluid should be constructed; 3) a non-Newtonian turbulent diffusion term should be determined; and 4) a contribution of viscosity fluctuations to the equation for the transport of the dissipation rate ε should be considered.

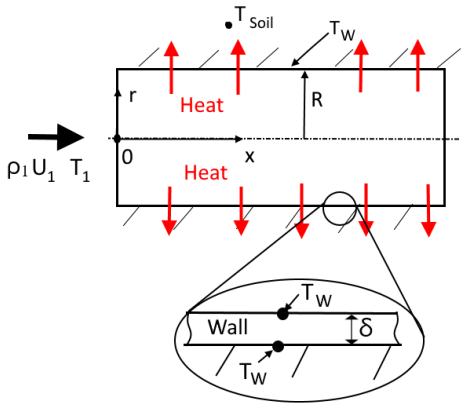

Fig. 1. Schematic of the flow configuration

Rheological Properties of a Non-Newtonian Fluid

In a non-Newtonian viscoplastic state, the effective molecular viscosity μ_{eff} can be modeled using the linear Bingham-Schwedoff rheological fluid model (De Kee, 2021). The effective molecular viscosity μ_{eff} of a fluid has the form (Bingham, 1922; Wilkinson, 1960; Klimov, et al., 2005):

$$\mu_{eff} = \begin{cases} \mu_p + \tau_0 \left|\dot{\gamma}\right|^{-1}, & \text{if } |\tau| > \tau_0 \\ \infty, & \text{if } |\tau| \le \tau_0 \end{cases}, \quad (1)$$

where $\tau_0 > 0$ is the yield shear stress, and μ_P is the plastic viscosity, $\boldsymbol{\tau} = \mu_{eff}\mathbf{S}$ is the shear stress tensor, and $\mathbf{S} \equiv \sqrt{2S_{ij} \cdot S_{ij}}$ is the strain rate tensor for instantaneous turbulent quantities and $S_{ij} = \frac{1}{2}\left(\frac{\partial U_i}{\partial x_j} + \frac{\partial U_j}{\partial x_i}\right)$ is the second invariant of the strain rate tensor. For a Newtonian fluid, the yield shear stress $\tau_0 = 0$ and the effective viscosity are constant and equal to the molecular viscosity of the corresponding fluid. The Bingham-Schwedoff model is a simple viscoplastic fluid model that linearly relates the yield shear stress to the viscosity (Bingham, 1922; Wilkinson, 1960; Klimov, et al., 2005).

The main difficulty in the numerical modeling of viscoplastic flows, including a turbulent regime, with the help of expression (1), is associated with the existence of a singular molecular viscosity in regions where the shear stress is less than τ_0. This difficulty is overcome by using various improvements of the basic rheological model (Bingham, 1922; Wilkinson, 1960; Klimov, et al., 2005). The approach of (Papanastasiou, 1987) was used in this work, where the effective viscosity was approximated by the following smooth function. It limits the value of effective viscosity as the shear rate tends to zero $\boldsymbol{\tau} \rightarrow 0$:

$$\mu_{eff} = \mu_p + \tau_0 \frac{\left[1-\exp\left(-10^3|\mathbf{S}|\right)\right]}{|\mathbf{S}|}. \quad (2)$$

The effective viscosity coefficient for a turbulent flow is the sum of the averaged coefficients of molecular viscosity μ and turbulent viscosity μ_T, similar to those of a Newtonian fluid (Iaccarino et al., 2010; Masoudian et al., 2016; Gavrilov & Rudyak, 2016; Pakhomov & Zhapbasbayev, 2021). The expression for the coefficient of the averaged dynamic viscosity of the turbulent non-Newtonian fluid considering (1), has the form:

$$\mu_{eff}^{T} = \left\langle \mu_{eff} \right\rangle + \mu_T = \mu_p + \tau_0 \left\langle |\mathbf{S}|^{-1} \right\rangle + \mu_T. \quad (3)$$

The averaged turbulent viscosity of the non-Newtonian fluid μ_T in Eq. (3) was determined in accordance with the turbulence model (Hwang & Lin, 1998) considering the appearance of the non-Newtonian behavior of the fluid using Eqs. (12–14) (see below). The viscosity of the non-Newtonian fluid in turbulent flows depends not only on the average turbulent velocity of the flow, but also on fluctuations of the shear rate tensor (Iaccarino et al., 2010; Masoudian et al., 2016; Gavrilov & Rudyak, 2016; Pakhomov & Zhapbasbayev, 2021). The instantaneous value of dynamic viscosity is represented as a sum of the averaged and pulsation components: $\hat{\mu} = \langle \mu \rangle + \mu'$. The expression for the mean shear rate in the non-Newtonian fluid has the following form and consists of two terms (Iaccarino et al., 2010; Masoudian et al., 2016; Gavrilov & Rudyak, 2016; Pakhomov & Zhapbasbayev, 2021):

$$\left\langle \mathbf{S}^2 \right\rangle = 2\left\langle S_{ij} \cdot S_{ij} \right\rangle = 2\left\langle S_{ij} \right\rangle \cdot \left\langle S_{ij} \right\rangle + 2\left\langle S_{ij}^{'} \cdot S_{ij}^{'} \right\rangle. \quad (4)$$

The variables in triangular brackets $\langle\ \rangle$ in Eq. (4) represent averaging, and the superscript (prime) refers to the fluctuation characteristics. The first term is determined by the gradients of the average flow velocity. The second one defines the averaged pulsation shear rate, and it is determined by the approach of (Gavrilov & Rudyak, 2016).

$$\rho\varepsilon = 2\left\langle S_{ij}^{'} \cdot S_{ij}^{'} \right\rangle \mu. \quad (5)$$

Then, the expression for the averaged shear rate (4) considering (5), based on the averaged viscosity model (Gavrilov & Rudyak, 2016), can be written as:

$$\langle \mathbf{S} \rangle = \sqrt{2\left\langle S_{ij} \right\rangle^2 + \left(\rho\varepsilon\right) / \langle \mu \rangle}. \quad (6)$$

The average effective molecular viscosity of the non-Newtonian turbulent fluid is related to the average shear rate by an expression similar to that used for defining for instantaneous turbulent quantities (1), i.e.:

$$\left\langle \mu_{eff} \right\rangle = \mu_p + \tau_0 \cdot \left\langle |\mathbf{S}|^{-1} \right\rangle. \quad (7)$$

Thus, the value of the average molecular viscosity of the turbulent Bingham-Schwedoff fluid can be predicted using Eqs. (6) and (7) and an iterative process. To determine the parameters of the current iteration when calculating the average strain rate, the effective viscosity was taken from the previous iteration: $\langle \mathbf{S} \rangle^{l} = \sqrt{2\left\langle S_{ij} \right\rangle^{2,\,l} + \left(\rho\varepsilon^{l}\right) / \langle \mu \rangle^{l-1}}$. The value of effective viscosity was then predicted on the new iteration layer: $\langle \mu \rangle^{l} = \mu_P^{l} + \tau_0^{l} \cdot \left\langle |\mathbf{S}|^{-1} \right\rangle^{l}$ and the process was repeated (Gavrilov & Rudyak, 2016).

The Governing Equations for a Non-Newtonian Non-Isothermal Turbulent Fluid

The governing equations are given in symbols of vector analysis operations, although they are solved for an axisymmetric flow in cylindrical coordinates. The set of steady-state axisymmetric RANS equations of continuity, momentum in axial and radial directions, and the energy of a turbulent incompressible generalized Newtonian fluid has the form:

$$\begin{aligned}
&\nabla \cdot \left(\rho \mathbf{U}\right) = 0 \\
&\nabla \cdot \left(\rho \mathbf{U}\mathbf{U}\right) = -\nabla P + \nabla \cdot \left(2\mu_{eff}\mathbf{S}\right) + \nabla \cdot \left(-\rho\left\langle \mathbf{u}'\mathbf{u}' \right\rangle\right) + \nabla \cdot \left\langle 2\mu_{eff}'\mathbf{S}' \right\rangle \\
&\nabla \cdot \left(\rho C_p T \mathbf{U}\right) = \nabla \cdot \left(\lambda \nabla T\right) + \nabla \cdot \left(-\rho C_p \left\langle \mathbf{u}' t' \right\rangle\right) + \boldsymbol{\tau} : \mathbf{S}.
\end{aligned} \quad (8)$$

Here, ρ, μ, λ, and C_P are the density, dynamic viscosity coefficient, thermal conductivity coefficient, and heat capacity of the fluid, respectively; $\mathbf{U} \equiv \left(u_x,\ u_r\right)$ is the velocity vector, ($u_x = U$, $u_r = V$) are the fluid velocity components in the axial (x) and radial (r) directions, respectively; P is the mean pressure; $\left\langle u_i u_j \right\rangle$ and $\left\langle u_j t \right\rangle$ are the Reynolds stress and turbulent heat flux. The last terms in the equations of motion and energy of system (8) consider the effects of heat release during viscous dissipation of kinetic energy in a non-Newtonian fluid (Beisembetov et al., 2016) and have the form (Beisembetov et al., 2016). The turbulent Reynolds stress $-\rho\left\langle \mathbf{u}'\mathbf{u}' \right\rangle$ and turbulent heat flux $-\rho C_p \left\langle \mathbf{u}' t' \right\rangle$ were written according to Boussinesq hypothesis. The expression $\nabla \cdot \left\langle 2\mu'_{eff}\mathbf{S}' \right\rangle$ in equation (8) is found according to representation of (Gavrilov & Rudyak, 2016).

In contrast to the RANS equations for a Newtonian fluid, the system of Eq. (8) contains additional terms representing the effect of the non-Newtonian behavior of the turbulent non-isothermal fluid. The fourth term on the right-hand side of the momentum equation describes the energy consumption of motion of a non-Newtonian fluid associated with an increase in viscosity and yield shear stress with a decrease in its temperature (Beisembetov et al., 2016). The second term on the right-hand side of the energy equation considers the heat release during the viscous dissipation of energy in a non-Newtonian fluid (Beisembetov et al., 2016).

It should be noted that all equations of set (9) were numerically solved in the form appropriate to an axisymmetric flow, but for brevity, they are given below in general Cartesian tensor form.

The Reynolds stress $\left\langle u_i u_j \right\rangle$ in the fluid phase was determined using the Boussinesq hypothesis:

$$-\rho\left\langle u_i u_j \right\rangle = 2\mu_T S_{ij} - \frac{2}{3}\rho k\delta_{ij} = \mu_T\left(\frac{\partial U_i}{\partial x_j} + \frac{\partial U_j}{\partial x_i}\right) - \frac{2}{3}\rho k\delta_{ij}, \tag{10}$$

where $\delta_{ij} = 1$ at $i = j$, and $\delta_{ij} = 0$ at $i \neq j$.

To build the mathematical model of the viscoplastic non-Newtonian fluid, it is necessary to establish a correlation between the deviators of the stress tensor and the strain rate tensor [35,36,39]:

$$\tau_{ij} = -\tau_0 + \mu_{eff}\left(\frac{\partial U_i}{\partial x_i} + \frac{\partial U_j}{\partial x_j}\right). \tag{11}$$

The turbulent heat flux in the non-Newtonian fluid was obtained according to the Boussinesq hypothesis, which have the form:

$$\rho\left\langle u_j t \right\rangle = -\frac{\mu_T}{\mathrm{Pr}_T}\frac{\partial T}{\partial x_j}. \tag{12}$$

Here, Pr_T is the turbulent Prandtl number. It was determined in accordance with (Kays, 1994), where it was shown that for the range of variation of the molecular Prandtl number Pr = 1–100, the turbulent Prandtl number was $\mathrm{Pr}_T = 0.85 + 0.7/\mathrm{Pe}_T$, where $\mathrm{Pe}_T = \mathrm{Pr}\left(\nu_T/\nu\right)$.

The Two-Equation Turbulence Model

$$\nabla\cdot\left(\rho\mathbf{U}k\right) = \nabla\cdot\left[\left(\mu_{eff} + \frac{\mu_T}{\sigma_k}\right)\nabla k\right] + 0.5\nabla\cdot\left(\mu\frac{k}{\tilde{\varepsilon}}\right)\nabla\varepsilon_W + \rho\left(\Pi_k - \varepsilon\right), \tag{13}$$

$$\nabla\cdot\left(\rho\mathbf{U}\tilde{\varepsilon}\right) = \nabla\cdot\left[\left(\mu_{eff} + \frac{\mu_T}{\sigma_\varepsilon}\right)\nabla\tilde{\varepsilon}\right] - \nabla\cdot\left(\mu\frac{\tilde{\varepsilon}}{k}\right)\nabla k - \frac{\rho\tilde{\varepsilon}}{k}\left(C_{\varepsilon 1}f_1\Pi_k + C_{\varepsilon 2}f_2\tilde{\varepsilon}\right), \tag{14}$$

$$\mu_T = C_\mu f_\mu \frac{\rho k^2}{\tilde{\varepsilon}}. \tag{15}$$

The system of equations of the turbulence model (Matvienko, 2011) resembles the equation system for a Newtonian fluid. The influence of non-Newtonian characteristics in the turbulence model was considered by the tensor of averaged shear rate. The averaged dynamic viscosity of a fluid depends not only on the

averaged, but also on the pulsation parameters of the turbulent non-Newtonian flow (Gavrilov & Rudyak, 2016).

Here k is the turbulent kinetic energy, $\tilde{\varepsilon}$ is the rate of its dissipation, and μ_T is the turbulent dynamic viscosity. The constants and damping functions in models (13)–(15) have the form [40]: C_μ = 0.09; $\sigma_k = 1.4 - 1.1\exp\left[-\left(0.1y_\lambda\right)\right]$; $\sigma_\varepsilon = 1.3 - \exp\left[-\left(0.1y_\lambda\right)\right]$; $C_{\varepsilon 1}$ = 1.44; $C_{\varepsilon 2}$ = 1.92; $f_1 = f_2 = 1$; $f_\mu = 1 - \exp\left(-0.01y_\lambda - 0.008y_\lambda^3\right)$; $y_\lambda = y/\sqrt{\nu k/\tilde{\varepsilon}}$ is the Taylor micro-scale; $\Pi_k = \mu_T\left(\frac{\partial U_i}{\partial x_j} + \frac{\partial U_j}{\partial x_i}\right)\frac{\partial U_i}{\partial x_j}$ is the turbulence production from the average motion; $\varepsilon = \tilde{\varepsilon} + \varepsilon_W$ is the full dissipation of gas turbulence energy; $\varepsilon_W = 2\nu\left(\frac{\partial\sqrt{k}}{\partial x_j}\right)^2$ is the value of TKE dissipation in the near-wall zone, and $\widehat{\mu}$ is the instantaneous value of dynamic viscosity of the non-Newtonian fluid (Gavrilov & Rudyak, 2016).

The Effect of Temperature on a Non-Newtonian Fluid

The non-isothermal fluid (waxy crude oil) has the properties of a Newtonian fluid (Beisembetov et al., 2016) at the pipe inlet. As a result of heat transfer with the surrounding cold medium through the pipe wall and a decrease in the flow temperature in its near-wall part, the effective viscosity increases, and yield shear stress appears. In a waxy crude oil this leads to the appearance of a non-Newtonian state. A decrease in the temperature of fluid can cause crystallization of the wax, and the release of the heat of the phase transition (Beisembetov et al., 2016; Zhao, 2020; Zhapbasbayev et al., 2021). The total amount of latent heat ΔH is defined by the form (Voller & Prakash, 1987):

$$C_P = \begin{cases} C_S, & t < t_S, \quad \text{in solid state,} \\ C_{Int}, & t_S \le t \le t_L, \quad \text{in transition zone,} \\ C_L, & t > t_L, \quad \text{in fliquid state,} \end{cases} \tag{16}$$

where C_S, C_L, and $C_{Int} = \left\{\int_{t_S}^{t_L} C_L(t)dt + \chi H_{1\to 2}\right\}/\left(t_L - t_S\right)$ are the thermal conductivity of wax in solid, liquid, and transition states, t_L and t_S are the initial and final values of the temperature of wax formation in the oil flow, χ is the wax fraction in the oil, $H_{1\to 2}$ is the specific enthalpy of the wax phase transition (Beisembetov et al., 2016). In Eq. (16): t_L = 32 ^{0}C, t_S = 22 ^{0}C, $H_{1\to 2}$ = 41.03 [kJ/kg], χ = 0.15.

The heat capacity C_L, plastic viscosity μ_P, yield shear stress τ_0, density ρ, and thermal conductivity λ of waxy crude oil as a function of temperature are described by empirical formulas of (Beisembetov et al., 2016):

$$C_L(t) = \left(53357 + 107.2\cdot t\right)/\sqrt{\rho_{20}}\ \text{, [J/(kg·°C)]}$$

$$\mu_P(t) = 0.3585\cdot\exp\left(-0.1792\cdot t\right)\text{, [Pa·s]}$$

$$\tau_0(t) = 589.56\cdot\exp\left(-0.567\cdot t\right)\text{, [Pa]}$$

$$\lambda(t) = 5.057\cdot\left(1 - 0.00054\cdot t\right)/\sqrt{\rho_{20}}\ \text{, [W/(m·°C)]}$$

$$\rho(t) = \rho_{20}\left[1 + \zeta\cdot\left(20 - t\right)\right]\text{, [kg/m}^3\text{]},$$

where ρ_{20} = 835 kg/m^3 is the fluid density at 20^{0}C and ζ = 0.000738, [1/^{0}C] is the coefficient of volumetric expansion. Table 1 presents the yield shear stress τ_0, and plastic viscosity μ_P vs fluid vs their temperature.

Table 1. The dependence of yield shear stress, and plastic viscosity of non-Newtonian fluid

***t*, ^{0}C**	***T*, *K***	**τ_0, Pa**	**μ_P, Pa·s**
0	273	589.6	0.3585
5	278	34.62044	0.14634
10	283	2.03286	0.05974

15	288	0.11937	0.02438
20	293	0.00701	0.00995
25	298	4.1156E-4	0.00406
30	303	2.41662E-5	0.00166

Boundary Conditions

No-slip conditions are set on the wall surface for the velocity and the condition of heat transfer with the environment medium is set for the temperature of the wall:

$$r = R = D/2:\ U = V = k = \tilde{\varepsilon} = 0 \text{ and } -\lambda_W \left(\frac{\partial T}{\partial r}\right)_W = \alpha_1 \left(T_m - T_W\right), \quad (17)$$

where r is the radial distance from the pipe axis, λ_W is the coefficient of thermal conductivity of the liquid determined from the wall temperature, h is the heat transfer coefficient from the oil flow in the pipe to the colder environment through the wall, $T_m = \frac{8}{U_{m1}D^2}\int_0^{D/2} T(r)U(r)rdr$ is the mean-mass temperature of the liquid in the considered cross-section, and the lower subscript "W" is the parameter determined according to the conditions on the pipe wall. The value of the heat transfer coefficient h from the fluid to the soil through pipe surface is determined by the formula (Beisembetov et al., 2016; Zhapbasbayev et al., 2021):

$$\frac{1}{hD} = \frac{1}{\alpha_1 D} + \sum_{i=1} \frac{1}{2\lambda_i} \ln \frac{D_{i+1}}{D_i} + \frac{1}{\alpha_2 D_2} \quad (18)$$

α_1 and α_2 are the "internal" and "external" heat transfer coefficients, D_1 and D_i are the inner and outer diameter of the pipe, and λ_i is the thermal conductivity of the pipe wall (stainless steel). The heat transfer coefficient α_1 is determined by considering the Fourier hypothesis for the heat flux:

$$\alpha_1 = \frac{-\lambda_W \left(\partial T / \partial y\right)_W D}{T_m - T_{W1}}, \quad (19)$$

The heat transfer coefficient α_2 is determined using the formula (Beisembetov et al., 2016):

$$\alpha_2 = \frac{2\lambda_{Soil}}{D_2 \ln\left[\frac{2H}{D_2} + \sqrt{\left(\frac{2H}{D_2}\right)^2 - 1}\right]}, \quad 20)$$

where λ_{Soil} is the thermal conductivity of the soil, and H is the depth of the pipe axis. The symmetry conditions are set on the pipe axis for all variables.

$$r = 0:\ \frac{\partial U}{\partial r} = \frac{\partial V}{\partial r} = \frac{\partial T}{\partial r} = \frac{\partial k}{\partial r} = \frac{\partial \tilde{\varepsilon}}{\partial r} = 0. \quad (21)$$

In the inlet section ($x = 0$), uniform distributions of velocity and temperature were specified over the cross-section of the pipe. At the outlet edge ($x = L$), the computational domain condition was set for all variables.

Thus, the system of equations (1)–(16) with the corresponding input and boundary conditions (17)–(21) is a closed system of equations that describes the processes of turbulent heat transfer in a waxy crude oil flow and allows the prediction of all the required quantities.

Numerical solution

The mean transport equations and the turbulence model were solved using a control volume method on a staggered grid. The QUICK scheme was used to approximate the convective terms, and the second-order accurate central difference scheme was adopted for the diffusion terms. The velocity correction was used to satisfy the continuity through the SIMPLEC algorithm, which couples the velocity and pressure.

All numerical simulations are performed using the "in-house" code. A non-uniform grid (in both axial and radial directions) was used and a grid refinement was applied in the inlet and the near-wall regions. The first cell was located at a distance in wall units $y_+ = yU_*/\nu = 0.3–0.5$ from the wall, where U_* is the friction velocity obtained for the flow in the inlet pipe, and ν is the kinematic viscosity. At least 10 control volumes

(CV) must be generated to resolve the mean velocity field and turbulence quantities in the viscosity-affected near-wall region ($y_+ < 10$). Grid sensitivity studies are commonly carried out to determine the optimum grid resolution that gives a mesh-independent solution. For all numerical investigations performed in this study, a basic grid with 1000×80 CV along the axial and radial directions was used. The part of the basic grid is given in the Fig. 2a. Grid convergence was verified for three grid sizes: coarse 750×50 and fine 1500×120 CV. The computational domain consisted of two sections and the length of each section is 10 m (x/D = 50). The conditions in the outlet of the first section were as the inlet conditions for the second one. Grid convergence is verified for three grid sizes is used for the "in-house" code: coarse 500×40, basic 1000×80 and fine 1500×120 CV control volumes (see Fig. 2b).

Differences in the value of TKE predicted for the non-Newtonian fluid flow is less than 0.1%. The maximum error $e_{\max}$ is defined as: $e_{\max} = \max_{i=1,\,N} \left| k_i^n - k_i^{n-1} \right| \le 10^{-6}$, where N is the total number of CVs in corresponding direction, the subscript i is the specific CV, and the superscript n is the iteration level. The computational grid is nonuniform both in the streamwise and transverse directions. The coordinate transformation is suitable for such a two-dimensional problem:

$\Delta\psi_j = K \times \Delta\psi_{j-1}$,

where $\Delta\psi_j$ and $\Delta\psi_{j-1}$ are the current and previous steps of the grid in the axial or radial directions and K = 1.08 (axial direction) and K = 1.05 (radial direction).

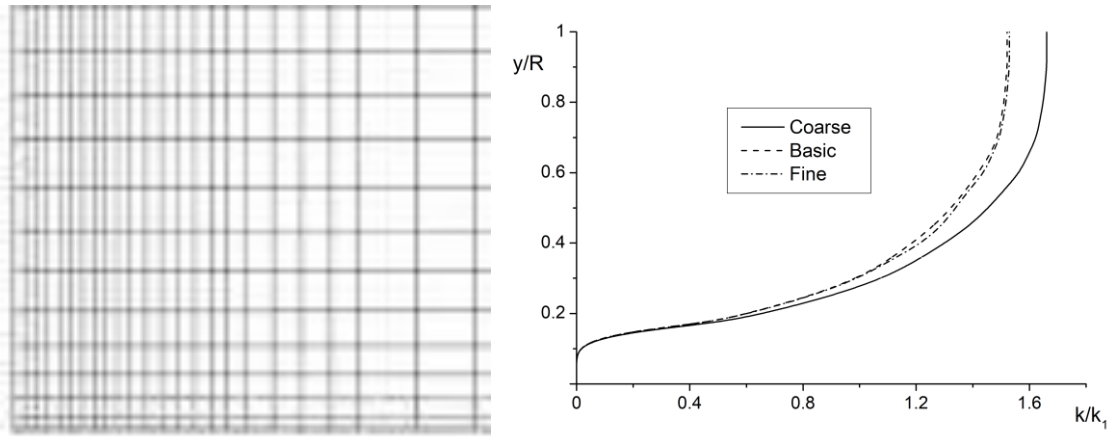

Fig. 2. Basic mesh grid (not in scale) (a) and grid convergence test (b) of "in-house" numerical code

Numerical results and discussion

A non-isothermal viscoplastic non-Newtonian fluid (waxy crude oil) flow along an underground pipe with an I.D. $D = 2R$ = 0.2 m, length L = 20 m (x/D = 100), and depth to pipe axis H = 2 m. The mean axial velocity and temperature profiles were uniform at the pipe inlet. All simulations were carried out in the region of hydrodynamic and thermal stabilization in a steady-state fluid flow in the pipe. Waxy crude oil in the inlet cross-section is considered as a Newtonian fluid. As fluid moves, the process of heat transfer through the pipe wall to the surround cold environment (soil) starts, and therefore the oil temperature is decreased. This leads to a sharp increase in viscosity and yield shear stress by decreasing of the fluid temperature. The velocity distribution will change both along the pipe length and along its cross-section

The profiles of dimensionless mean axial velocity U/U_{m1} (a), kinetic energy of turbulence k/k_1 (b), temperature $\Theta = (T - T_{W1}) / (T_1 - T_{W1})$ (c), average dynamic viscosity $\mu_{eff}/(\mu_T+\mu)$ (d), and yield shear stress $\tau_0/\tau_{0,1}$ (e) are shown in Fig. 3. Here, $y = R–r$ is the distance from the wall, R is the pipe radius, r is the radial distance from the pipe axis, μ represents the molecular viscosity of a Newtonian fluid (waxy oil), and $\tau_{0,1}$ is the yield shear stress at T = 293 K. The profiles of all parameters considered were uniform at the pipeline inlet (line *1*).

The inlet profile of the mean longitudinal velocity component was significantly deformed due to the process of heat transfer of the fluid with the soil environment through the pipe wall (see Fig. 3a). The value of the axial velocity was zero and it increased and reaches its maximum value in the axial region on the pipe wall.

The values of the longitudinal velocity in the axial zone increased as the fluid moved along the pipe length. On the contrary, it decreased in the near-wall zone. The value of the mean axial fluid velocity in the axial region of the pipe increased by more than 1.6 times in comparison with the inlet velocity. The transverse profiles of fluid turbulence also underwent significant changes as the fluid moved along the pipe length (see Fig. 3b). An increase in the level of turbulent kinetic energy in the axial zone of the pipe (by more than 1.5 times) and its noticeable decrease in its near-wall region were observed, which was associated with the corresponding changes in the profile of the mean longitudinal velocity (see Fig. 3a). Fluid turbulence is determined by the known relationship for an axisymmetric flow:

$$2k = \left\langle u'^2 \right\rangle + \left\langle v'^2 \right\rangle + \left\langle w'^2 \right\rangle \approx \left\langle u'^2 \right\rangle + 2\left\langle v'^2 \right\rangle.$$

It should be noted that the use of an isotropic two-parameter $k-\tilde{\varepsilon}$ model (Rudman & Blackburn, 2006), written with partial consideration of the rheological properties of a non-Newtonian fluid, has limitations when simulating turbulent non-Newtonian flows. This is explained by the significant anisotropy of the components of the Reynolds stress tensor in non-Newtonian flows (Masoudian et al., 2020; Gavrilov & Rudyak, 2016). Therefore, this approach is the first step towards to describing the fluid flow and heat transfer in turbulent non-Newtonian flows.

The flow of waxy crude oil was originally a Newtonian fluid at the pipe inlet. Then, it cooled via heat transfer with the soil environment through the pipe wall. The decrease in the temperature of the fluid (see Fig. 3c) led to a change in its rheological and physicochemical properties and viscoplastic properties began to appear (De Kee, 2021; Bingham, 1922; Wilkinson, 1960; Klimov, et al., 2005). Therefore, with a decrease in the fluid temperature in the near-wall zone during heat transfer with the wall, the values of the average dynamic viscosity coefficient $\mu_{eff} = \mu_P+\mu_T+\mu$ (see Fig. 1c) and the yield stress τ_0 (see Fig. 3d) increased significantly.

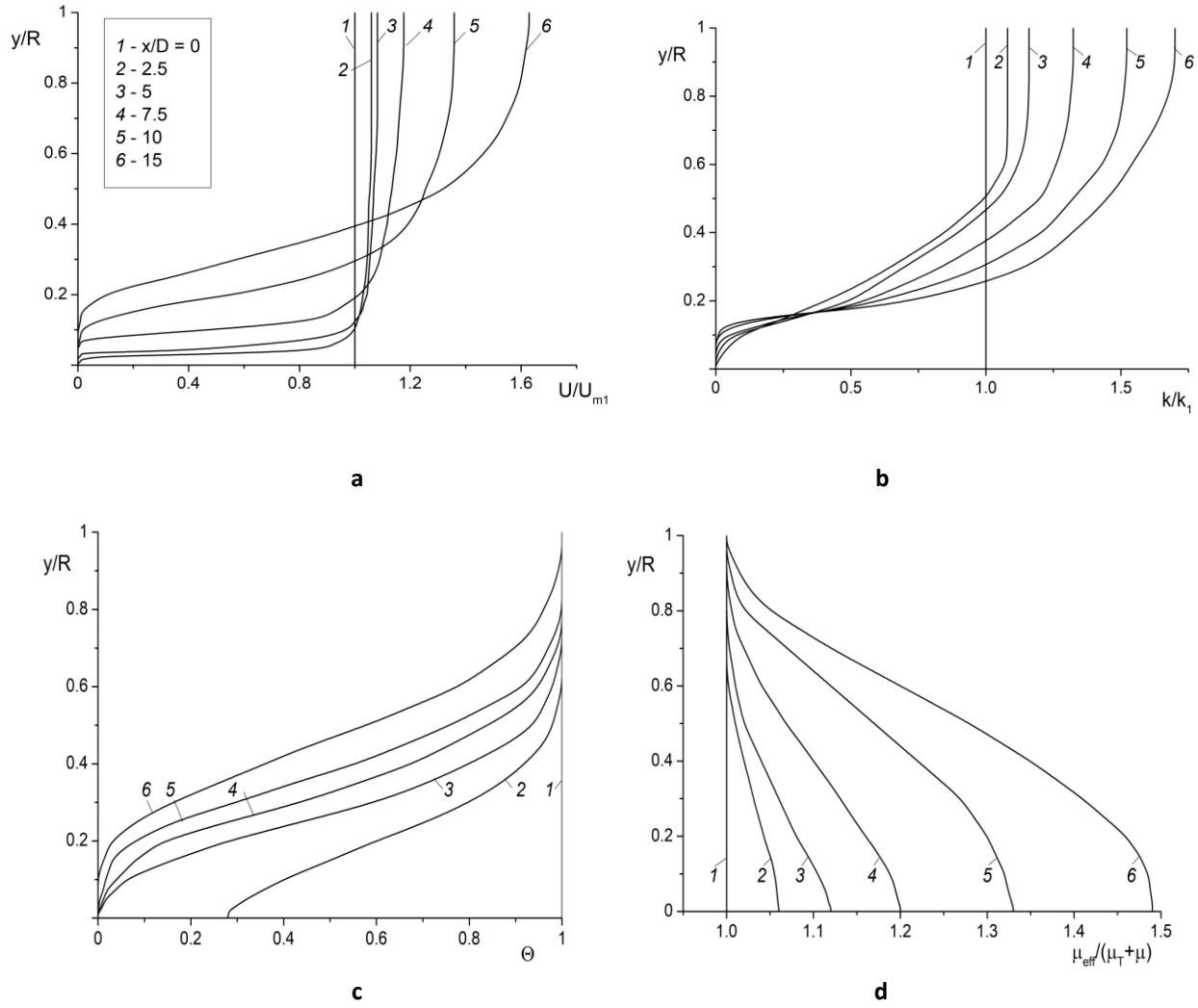

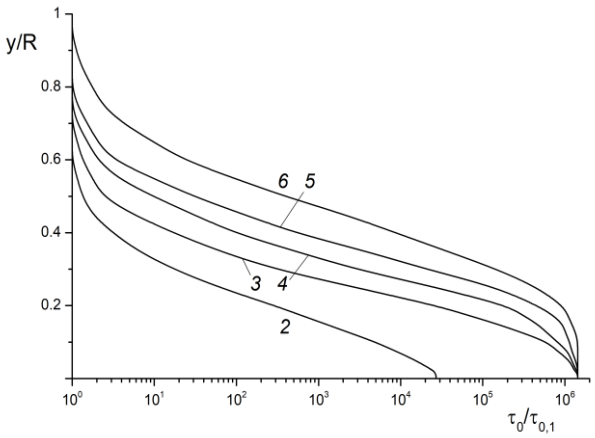

e

Fig. 3. Radial profiles of dimensionless distributions of mean axial velocity (a), turbulent kinetic energy (b), temperature (c), averaged effective dynamic viscosity (d), and yield shear stress (e). D = 0.2 m, U_{m1} = 0.2 m/s T_1 = 298 K, T_{Soil} = 273 K

These two figures give clear information about the effect of non-Newtonian (viscoplastic) behavior on the fluid flow. It is known (Chala et al., 2018; Elkatory et al., 2022; Zhao, 2020) that at temperature $T \leq 293$ K, the yield shear stress τ_0 appears in the near-wall zone (see Fig. 3d), and this also leads to the velocity deceleration of the turbulent non-Newtonian fluid. It is obvious that with a decrease in the flow through the cross-section of the pipe with a constant mass flow rate of fluid along the pipe length, the axial velocity should increase, which is observed in Fig. 3a. The size of the near-wall section with a lower temperature increased towards the pipe axis and through the movement of fluid along the pipe length. This led to an increase in the average dynamic viscosity of the waxy crude oil and the yield shear stress.

The radial profiles of temperature, and the average dynamic viscosity along the pipe length show that waxy crude oil had the properties of a Newtonian fluid over the cross-section of the pipe in the temperature range $T \geq 293$ K, while in the temperature range $T < 293$ K, it had the properties of a viscoplastic (non-Newtonian) fluid. This is in qualitative agreement with the data of numerical calculations for the laminar flow of non-Newtonian fluids in a pipe (Zhao, 2020). Therefore, it seems important to determine the boundaries of existence of the Newtonian properties of a turbulent non-isothermal flow of waxy oil.

The results of numerical predictions on the effects of the surrounding environment's temperature T_{Ssoil} on the distributions of dimensionless mean axial velocity (a), kinetic energy of turbulence (b), coefficient of average dynamic viscosity (c), yield shear stress (d), and Reynolds stresses (e) over the pipe cross-section are presented in Fig. 4. The viscoplastic properties in distributions of the mean longitudinal velocity, turbulent kinetic energy, average viscosity, and yield shear stress, characteristic of the Bingham-Schwedoff fluid, were most clearly revealed at ambient temperature T_{Soil} = 273 K (*1*). The fluid flow characteristics at T_{Soil} = 298 K (*3*) fully agree with simulations for the Newtonian fluid with other conditions being identical. The profiles of the axial velocity had a form characteristic of the flow in the section of hydrodynamic stabilization (see Fig. 4a). The fluid turbulence had a characteristic maximum located in the near-wall region of the pipe (see Fig. 4b). The dynamic viscosity did not differ from the viscosity of a turbulent flow of a Newtonian fluid (see Fig. 4c). The yield shear stress was completely absent (see Fig. 4d). The prediction at T_{Soil} = 288 K (*2*) was characterized by the fact that the viscoplastic properties of the fluid were already beginning to appear.

The dimensionless Reynolds stresses $\langle uv \rangle_+ = \langle uv \rangle / u_*^2$ in the fluid are shown in Fig. 4e with varying temperatures of the surrounding soil, where u_* is the wall friction velocity for a Newtonian fluid. Reynolds stress for the axisymmetric flow were calculated by the relationship $\langle u_i u_j \rangle = -\nu_T \left(\frac{\partial U_i}{\partial x_j} + \frac{\partial U_j}{\partial x_i} \right) + \frac{2}{3} k \delta_{ij}$. A decrease in the temperature of the surrounding soil had a noticeable effect on the level of Reynolds stress. The Reynolds stress in the flow of the non-Newtonian fluid (*2* and *3*) were noticeably higher than the corresponding value for a Newtonian fluid (*1*), with all other conditions being identical. In the near-wall and axial parts of the pipe, the Reynolds stress were equal to zero, since in these parts of the pipe the velocity

gradient and the level of turbulent kinetic energy were equal to zero (see Figs. 3a and 3b). The maximum Reynolds stress occurred in the near-wall part of the pipe for the whole investigated temperature range and there was a shift in the position of the maximum towards the pipe axis with a decrease in the temperature of the fluid. For example, for a Newtonian fluid at T_{Soil} = 298 K, the position of maximum was at a distance $y/R \approx 0.1$, while for T_{Soil} = 273 K the coordinate $y/R \approx 0.2$. This was explained by an increase in the thickness of the near-wall layer with the appearance of yield stresses.

Changes in the position of the points of mean axial flow velocity $U = 0$ (*1*), velocity $U = U_{m1}$ (*2*), and liquid temperature T = 293 K (*3*) and 298 K (*4*) along the pipe length are shown in Fig. 5. The solid lines (*1* and *2*) refer to the axial mean velocities of the fluid and the dashed lines (*3* and *4*) refer to the temperatures. The value of longitudinal velocity of fluid on the pipe wall was always zero, but in this case, line *1* in Fig. 5 shows the upper boundary of existence of the zone with a zero fluid flow velocity from the pipe wall. The height of the region with a zero fluid velocity in the pipe increased gradually as the waxy crude oil moved along the pipe length and reached $y/R \approx 0.55$ at x/D = 100 (x = 20 m). The position of the point where the fluid velocity was equal to the velocity in the inlet cross-section $U = U_{m1}$ (*2*) shifted gradually towards the pipe axis and $y/R \approx 0.9$ at x/D = 100. This was related to an increase in the fluid velocity in the flow core due to flow deceleration in the near-wall part of the pipe. It should be noted that the value of maximum fluid velocity in the axial region of the pipe increased significantly, while in its near-wall part it decreased due to flow cooling (see Fig. 5a).

The height of the region with the fluid temperature T = 293 K (*3*) shifted towards the pipe axis as it moved along the pipe length and reached $y/R \approx 1$ at x/D = 100. In terms of its physical implications, this was the upper boundary of the area of existence of the non-Newtonian fluid behavior. The yield shear stress in waxy crude oil (Bingham-Schwedoff viscoplastic non-Newtonian fluid) appears at t = 20°C and this value of temperature is a threshold for yielded and unyielded regions. In the region with temperature T = 298 K (*4*), this region also shifted towards the pipe axis and y/R = 1 at x/D > 50. This confirms the data of our numerical predictions, shown in Fig. 3, on the significant effect of fluid temperature on the processes of turbulent transport of momentum and heat in a non-Newtonian Bingham-Schwedoff fluid.

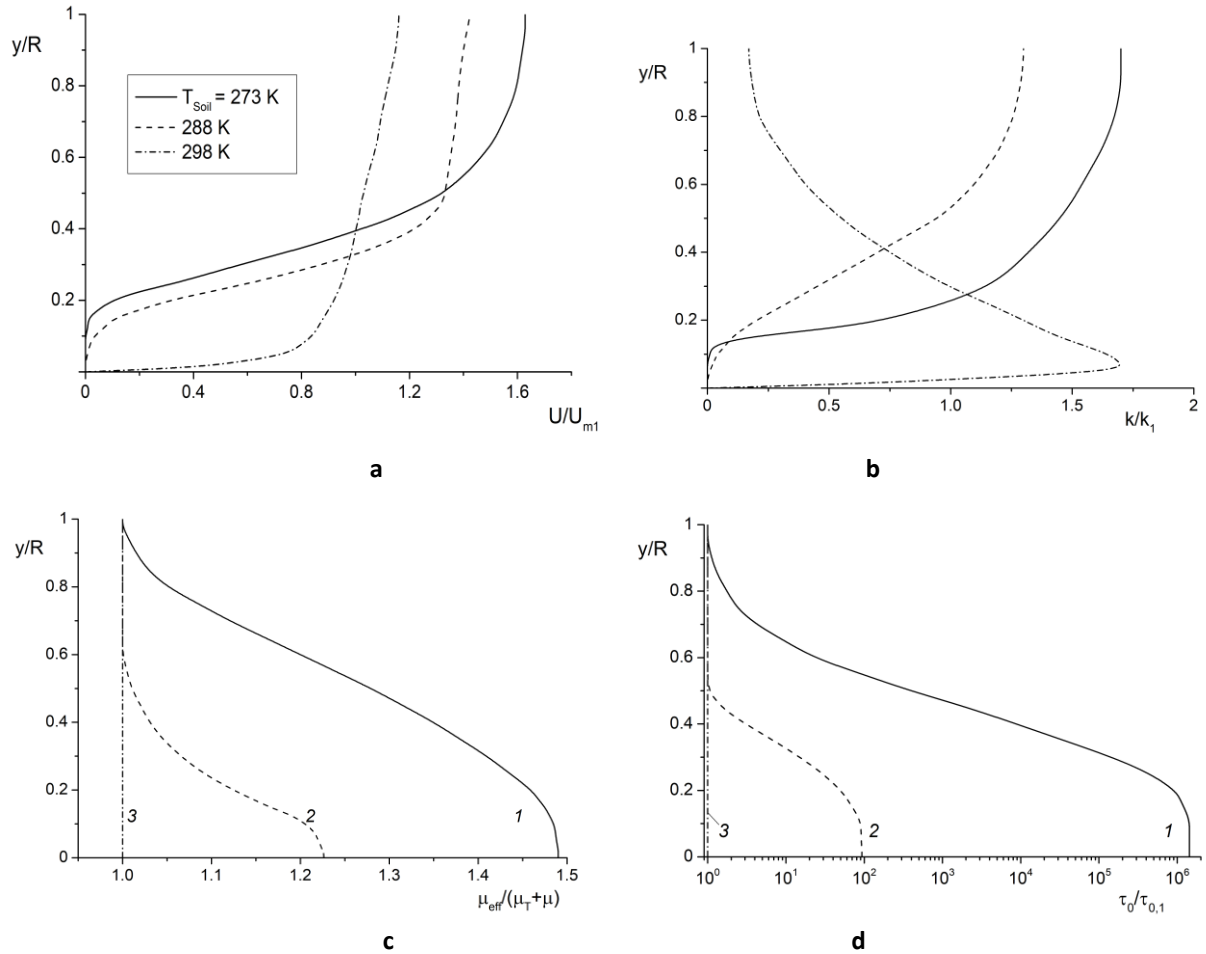

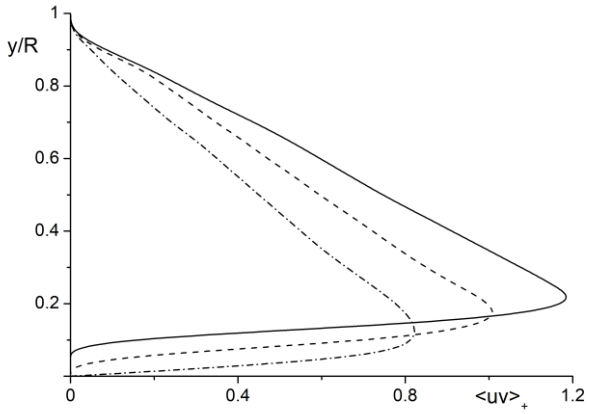

E

Fig. 4. The dimensionless mean axial velocity (a), turbulent kinetic energy (b), average effective dynamic viscosity (c), yield shear stress (d), and Reynolds stress (e) plotted for different soil temperatures. x/D = 15, x = 3 m

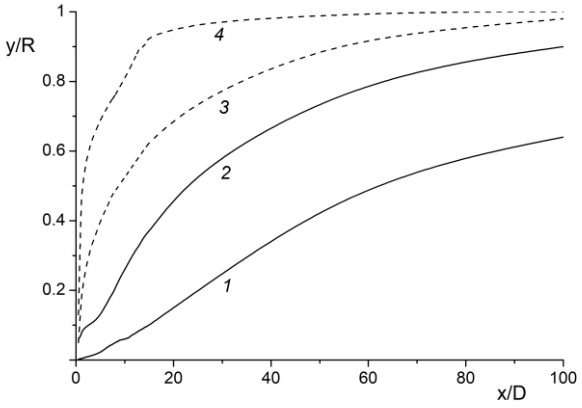

Fig. 5. The distributions along the pipe length of mean axial velocity of the flow equal U = 0 (*1*), mean axial velocity of the flow equal $U = U_{m1}$ (*2*), and temperatures equal T = 293 K (*3*) и T = 298 K (*4*). T_1 = 298 K, T_{Soil} = 273 K

The contour plots of the mean axial velocity (a), temperature (b), kinetic energy (c), and average effective dynamic viscosity (d) in the are given in the Fig. 6. These contours clearly show the main features of turbulent motion and heat transfer in the turbulent non-isothermal non-Newtonian fluid and they confirm the main conclusions in the abovementioned Figures 3–5. There is no flow motion in the "bottom" direction from the line U/U_{m1} = 0 and the flow accseleration is obtained in the "upper" direction from the line U/U_{m1} = 1 (see Fig. 6a). The behavior of the Newtonian fluid is observed in the "upper" zone from the line T = 298 K, and the line T = 293 K is the lower bundary for the existence of the yeld shear stress (see Fig. 6b). In the "upper" direction from the line k/k_1 = 1 is predicted the additional turbulence production due to the flow accseleration (see Fig. 6c). The line of average effective dynamic viscosity $\mu_{eff}/(\mu_T+\mu_1)$ = 1 is the "lower" boundary for the existence of the properties of the Newtonian fluid (see Fig. 6d).

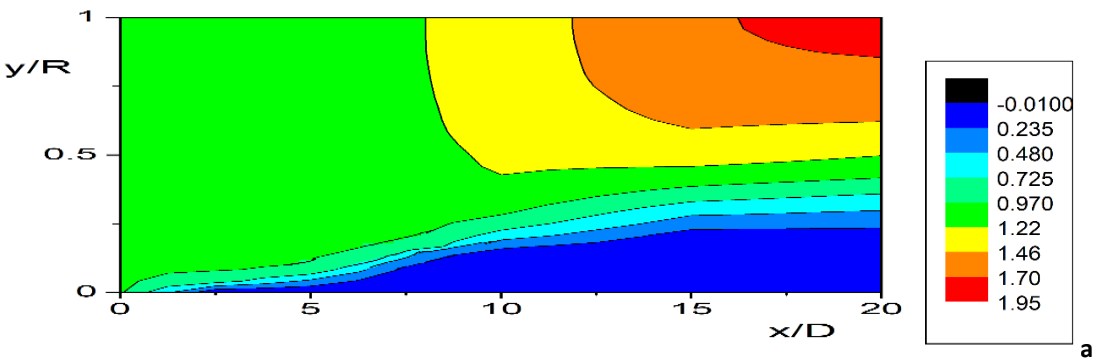

a

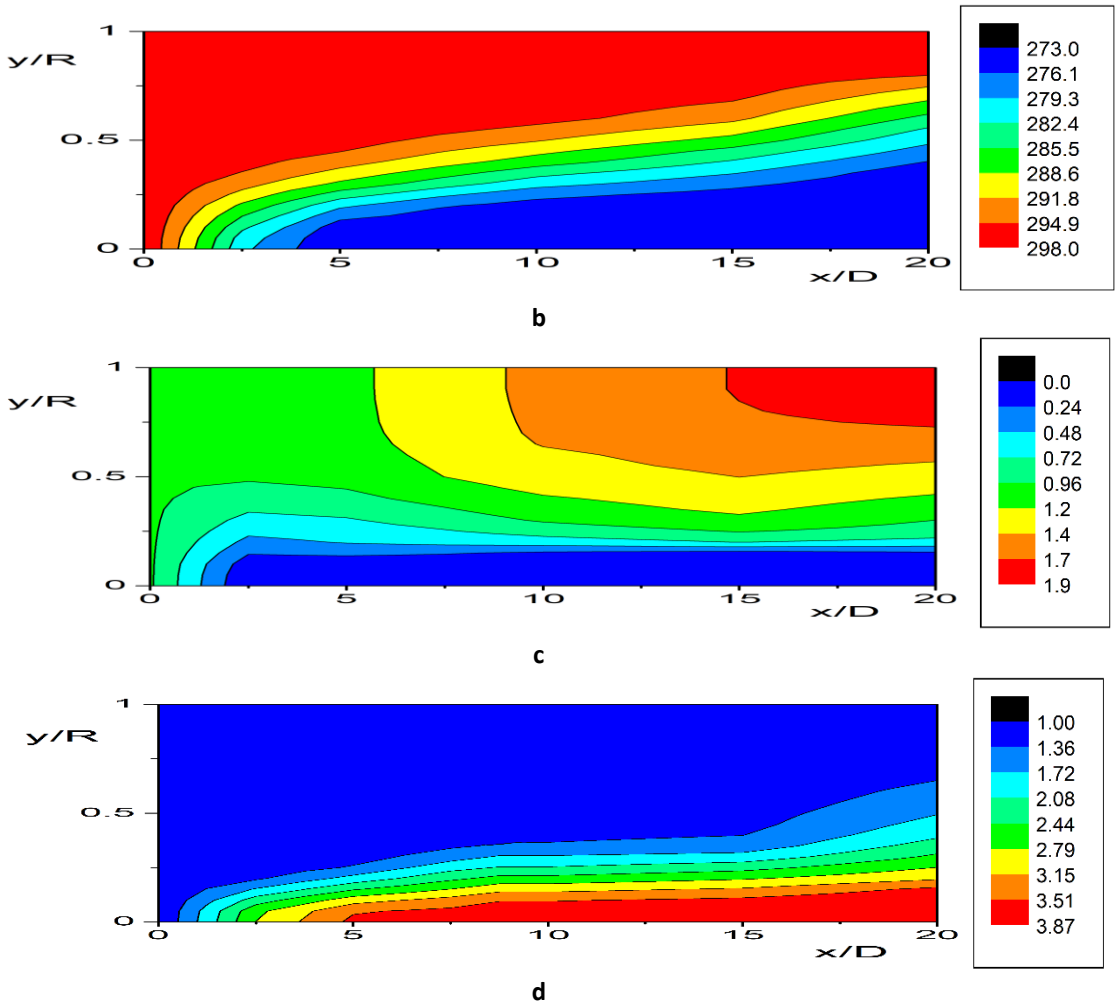

Fig. 6. Contours plots of mean axial velocity U/U_{m1} (a), mean temperature T, K (b), turbulent kinetic energy k/k_1 (c), and average effective dynamic viscosity $\mu_{eff}/(\mu_T+\mu_1)$ (d). The transverse height of the plots is not in the scale. U_{m1} = 0.2 m/s, T_1 = 298 K. T_{Soil} = 273 K, Re = 8200

Comparison with results of other authors for laminar and turbulent non-newtonian fluids

Turbulent Isothermal Non-Newtonian Flow

Fig. 7 shows a comparison of DNS data (Singh et al., 2017) and RANS predictions by the author for the distributions of dimensionless axial velocity $U_+ = U/u_*$ (a) and kinetic energy of turbulence $k_+ = k/u_*^2$ (b) in universal wall coordinates $y_+ = \rho u_* y/\mu_W = \rho u_* (R-r)/\mu_W$ for a Newtonian fluid (*1* and *3*) and for a turbulent Bingham-Schwedoff fluid (*2* and *4*). Here, *R* is the pipe radius and *r* is the current radial coordinate. The solid points represent the DNS data (Singh et al., 2017) and the lines are the author' predictions. The logarithmic velocity profile is also shown in Fig. 7a.

In the viscous (y_+ <5) and buffer (5 < y_+ < 30) areas, the simulations for a turbulent Newtonian and the non-Newtonian fluids gave almost the same values and there was a good quantitative agreement with the data of (Singh et al., 2017) (see Fig. 7a). It could be concluded that a change in the yield shear stress was not observed within the viscous sublayer and the difference between non- and Newtonian fluids was minimal. According to the distributions of axial velocities, an excess was noted according to the RANS computations (up to 10%) in comparison with the DNS data in the logarithmic layer (30 < y_+ < 200). In the logarithmic layer (lines *2* and *4*), this difference did not exceed 10%, and the author's velocity profile was similar to that of a Newtonian fluid.

Distributions of turbulent kinetic energy predicted by the author also agreed satisfactorily with the DNS data (Singh et al., 2017) in the viscous sublayer and in the logarithmic region (the difference did not exceed 15%) (see Fig. 9b). Here NF and NNF are the Newtonian and non-Newtonian fluids respectively. As well as for DNS, in the logarithmic layer at y_+ = 10–55, an additional generation of turbulence in the Bingham-Schwedoff fluid was shown as a comparison to the Newtonian fluid (an excess of up to 10%). Whereas, for y_+ > 100, the

results of DNS results showed the opposite: an insignificant suppression of turbulent kinetic energy (no more than 5–7%), which was not predicted by the author's RANS model. The authors of (Singh et al., 2017) explained this by a change in the ratio between longitudinal and transverse pulsations. The position of the peak in the turbulence level according to the RANS data was shifted towards the pipe axis (by 20%) in comparison with the DNS data (Singh et al., 2017) for both types of investigated fluids. The position of TKE maximum by DNS was $y_+ \approx 16$, and according to RANS computations, it was $y_+ \approx 20$.

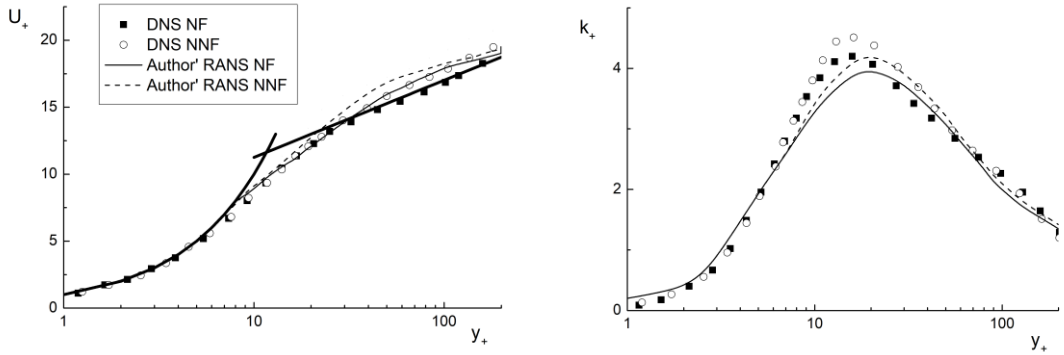

Fig. 7. The mean axial flow velocity (a), and turbulence (b) plotted in wall coordinates for turbulent Newtonian (*1* and *3*), and BS (*2* and *4*) fluids respectively. Points are DNS of (Singh et al., 2017), curves are author' RANS simulations. Re = 1.1×10^4, $Re_\tau = 323$, $U_{m1}/u_* = 16.24$, $\tau_0/\tau_W = 1.1$

Comparison of DNS (Singh et al., 2017) and our RANS calculations for dimensionless distributions of axial velocity pulsations (a) and pulsation (b) for Newtonian fluid (lines *1* and *3*) and for Bingham-Schwedoff turbulent fluid (*2–6*) is shown in Fig. 8. In Fig. 8 points are DNS (Singh et al., 2017), lines are RANS calculation of authors using $k–\tilde{\varepsilon}$ model [36], Re = $U_{m1}D_1/\nu_{W1} = 1.3\times10^4$, $Re_\tau = u_*R_1/\nu_W = 323$. Lines *1* and *3* are Newtonian fluid; curves *2* and *4* are non-Newtonian fluid $\tau_0/\tau_W = 1.1$; lines *3* and *6* are non-Newtonian fluid at $\tau_0/\tau_W = 1.2$. The axial (see Fig. 8a) and the radial (see Fig. 8b) velocity pulsation profiles show differences with the DNS (Singh et al., 2017). The axial and radial components of the Reynolds stresses are typically determined in the isotropic $k–\tilde{\varepsilon}$ model: $u' = v' = 2k/3$. The axial averaged velocity profile along the tube cross section is qualitatively similar to the one for a Newtonian fluid. This is characteristic both for the DNS (Singh et al., 2017) and for our RANS calculations. However, the isotropic $k–\tilde{\varepsilon}$ model (Matvienko et al., 2011) does not even qualitatively describe the complex distribution of velocity pulsations over the pipe cross section and significant anisotropy of axial and radial velocity pulsations of BS fluid. This is especially noticeable in the profiles of the radial velocity pulsations (see Fig. 8b).

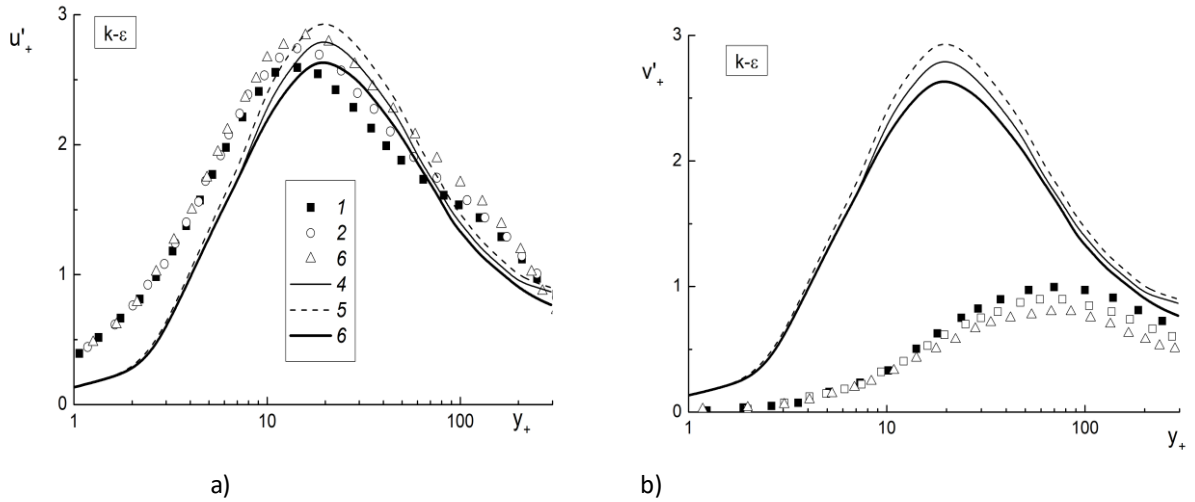

Fig. 8. Comparison of the results of RANS calculations of axial $u'_+ = u'/u_*$ (a) and radial $v'_+ = v'/u_*$ (b) velocities fluctuations. Points *1–3* are the DNS (Singh et al., 2017), lines *4–6* are authors' simulations; *1* and *5* are the Newtonian fluid; *2* and *4* are the non-Newtonian fluid $\tau_0/\tau_W = 1.1$; *3* and 6 are the non-Newtonian BS fluid $\tau_0/\tau_W = 1.2$

Conclusions

A numerical model for the simulation of the turbulent fluid flow and heat transfer of a non-Newtonian Bingham-Schwedoff fluid has been developed. The mathematical model is based on a RANS approach with considerations of the non-Newtonian behavior of the fluid. Fluid turbulence was described using the isotropic two-parameter k–$\tilde{\varepsilon}$ model.

The Newtonian properties of fluid in the initial cross-sections of the pipe transformed gradually into a viscoplastic non-Newtonian fluid state due to heat transfer between the heated fluid in the pipe with a cold environment through the pipe wall. The value of axial velocity in the axial zone increased (up to 1.6 times in comparison with the velocity profile at the inlet), while in the near-wall zone, on the contrary, it decreased, and the height of the region with zero fluid velocity increased. A significant increase in the level of turbulent kinetic energy in the axial zone of the pipe (by more than 1.5 times) was noticed alongside its decrease in the near-wall region. The boundary of the area of existence of Newtonian properties of fluid was determined. It was found that the height of a region with fluid temperature $T \geq 293$ K decreased along the pipe length and it was $y/R \approx 0.6$ at $x/D = 15$. A significant increase in the average dynamic viscosity and yield stress in the near-wall part of the pipe was shown.

The characteristics of a turbulent isothermal Bingham-Schwedoff fluid within a viscous sublayer almost did not differ from the main Newtonian fluid regularities. In the logarithmic layer, the velocity profile for the non-Newtonian fluid had a form qualitatively similar to that of the Newtonian fluid. An excess of the axial velocity was characteristic for both types of non-Newtonian fluids with a logarithmic profile.

Funding

This work supported by the Science Committee of the Ministry of Science and Higher Education of the Republic of Kazakhstan (Grant number AP14869322 for 2022-2024).

Note

The main results are published in a paper published in the book Research and Development in Engineering Research, 2023. Vol. 5, 30 June 2023, Chapter 10, pp. 165-192.
https://doi.org/10.9734/bpi/rader/v5/5955EPublished: 2023-06-30

Cite this article as: Pakhomov M.A., Zhapbasbayev U.K. RANS modeling of the transition of a non-isothermal flow of a Newtonian fluid to a viscoplastic state in a pipe. *Challenges of Science*. Issue VI, 2023, pp. 108-123. https://doi.org/10.31643/2023.13

References

Aiyejina A., Chakrabarti D.P., Pilgrim A., Sastry M.K.S. (2011). Wax formation in oil-pipelines: a critical review. International Journal Multiphase Flow, Vol. 37(7), pp. 671–694.

Amani E., Ahmadpour A., Aghajari M.J. (2023). Large-Eddy Simulation of Turbulent Non-Newtonian Flows: A Comparison with State-of-the-Art RANS Closures. International Journal Heat Fluid Flow. Vol. 99, 109076.

Barnes H.A. (1999). The Yield Stress−A Review or 'παντα ρει'−Everything Flows? Journal Non-Newtonian Fluid Mechanics. Vol. 81(1-2), pp. 133–178.

Beisembetov I.K., Bekibayev T.T., Zhapbasbayev U.K., et al. (2016). Management of Energy-Saving Modes of Oil Mixtures Transportation by the Main Oil Pipelines, Almaty: Publ. House of KBTU.

Bingham E.C. (1922). Fluidity and Plasticity, New York: McGraw-Hill.

Bostanjiyan S.A., Chernyaeva S.M. (1966). On the Hydrodynamic Thermal "Explosion" of Non-Newtonian Fluid. Reports Academy Sci. USSR, Vol. 170(2), pp. 301–304 (in Russ.).

Chala G.T., Sulaiman S.A. (2018). Japper-Jaafar A. Flow start-up and transportation of waxy crude oil in pipelines−a review. Journal Non-Newtonian Fluid Mechanics. Vol. 251, pp. 69–87.

Cruz D.O.A., Pinho F.T. (2003). Turbulent Pipe Flow Predictions with a Low Reynolds Number k-ε Model for Drag Reducing Fluids. Journal Non-Newtonian Fluid Mechanics, Vol. 114(2-3), pp. 109–148.

Danane F., Boudiaf A., Mahfoud O., Ouyahia S.-E., Labsi N., Benkahla Y.K. (2020). Effect of Backward Facing Step Shape on 3D Mixed Convection of Bingham Fluid, International Journal Thermal Sciences, Vol. 147, 106116.

De Kee D. (2021). Yield Stress Measurement Techniques: A Review. Phys. Fluids, Vol. 33, 111301.

Elkatory M.R., Soliman E.A., E.l. Nemr A., Hassaan M.A., Ragab S., El-Nemr M.A., Pantaleo A. (2022). Mitigation and Remediation Technologies of Waxy Crude Oils' Deposition within Transportation Pipelines: A Review. Polymers, Vol. 14, 3231.

Gavrilov A.A., Rudyak V.Ya. (2017). Direct Numerical Simulation of the Turbulent Energy Balance and the Shear Stresses in Power-Law Fluid Flow in a Pipe. Fluid Dynamics. Vol. 52(3), pp. 363–374.

Gavrilov A.A., Rudyak V.Ya. (2016). Reynolds-averaged modeling of turbulent flows of power-law fluids. Journal Non-Newtonian Fluid Mechanics, Vol. 227, pp. 45–55.

Ghannam M.T., Hasan S.W., Abu-Jdayil B., Esmail N. (2012). Rheological Properties of Heavy & Light Crude Oil Mixtures for Improving Flow Ability. Journal Petroleum Science Engineering, Vol. 81, pp. 122–128.

Gnambode P.S., Orlandi P., Ould-Rouiss M., Nicolas X. (2015). Large-Eddy Simulation of Turbulent Pipe Flow of Power-Law Fluids. International Journal Heat Fluid Flow, Vol. 54, pp. 196–210.

Hussain H.H., Sulaiman S.A., Chala G.T., Husin H. (2023). Effect of Crude Oil and Nitrogen Gas Flow Rates on the Time Taken for Flow Initiation of Waxy Crude Oil. Processes, Vol. 11, 1414.

Hwang C.B., Lin C.A., (1998). Improved Low-Reynolds-Number k–$\tilde{\varepsilon}$ Model Based on Direct Simulation Data. AIAA Journal, Vol. 36(1), pp.38–43.

Iaccarino G., Shaqfeh E.S.G., Dubief Y. (2010). Reynolds-Averaged Modeling of Polymer Drag Reduction in Turbulent Flows. Journal Non-Newtonian Fluid Mechanics, Vol. 165(7-8), pp. 376–384.

Kays M. (1994). Turbulent Prandtl Number – Where We Are? ASME Journal Heat Transfer, Vol. 116(2), pp. 284–295.

Klimov D.M., Petrov A.G., Georgievsky D.V. (2005). Viscoplastic Flows: Dynamic Chaos, Stability and Mixing, Moscow: Publ. House Nauka (in Russ.).

Lovato S., Keetels G.H., Toxopeus S.L., Settels J.W. (2022). An Eddy-Viscosity Model for Turbulent Flows of Herschel–Bulkley Fluids. Journal Non-Newtonian Fluid Mechanics, Vol. 301, 104729.

Malin M.R. (1997). The Turbulent Flow of Bingham Plastic Fluids in Smooth Circular Tubes. International Communication Heat Mass Transfer, Vol. 24(6), pp. 793-804.

Masoudian M., Pinho F.T., Kim K., Sureshkumar R. (2016). A RANS Model for Heat Transfer Reduction in Viscoelastic Turbulent Flow. International Journal Heat Mass Transfer. Vol. 100, pp. 332–346.

Matvienko O.V., Bazuev V.P., Yuzhanova N.K. (2011). Mathematical Simulation of a Twisted Pseudoplastic Fluid Flow in a Cylindrical Channel. Journal Engineering Physics Thermophysics, Vol. 84(3), pp. 589–593.

Pakhomov M.A., Zhapbasbayev U.K. (2021). RANS Modeling of Turbulent Flow and Heat Transfer of Non-Newtonian Viscoplastic Fluid in a Pipe. Case Studies Thermal Engineering, Vol. 28, 101455.

Papanastasiou T.C. (1987). Flows of Materials with Yield. Journal Rheology, Vol. 31(5), pp. 385–404.

Rudman M., Blackburn H.M. (2006). Direct Numerical Simulation of Turbulent Non-Newtonian Flow Using a Spectral Element Method. Applied Mathematical Modelling, 30(11), pp. 1229−1248.

Sahu K.C., Valluri P., Spelt P.D.M., Matar O.K. (2007). Linear instability of pressure-driven channel flow of a Newtonian and a Herschel-Bulkley fluid. Physics Fluids, Vol. 19(12), 122101.

Singh J., Rudman M., Blackburn H.M. (2017). The Effect of Yield Stress on Pipe Flow Turbulence for Generalised Newtonian Fluids, Journal Non-Newtonian Fluid Mechanics, Vol. 249, pp. 53−62.

Tugunov P.I., Novoselov V.I. (1972). Transportation of Viscous Oil and Petroleum Products Through Pipelines, Moscow: Publ. House Nedra. (in Russ.).

Usha R., Sahu K.C. (2019). Interfacial instability in pressure-driven core-annular pipe flow of a Newtonian and a Herschel-Bulkley fluid. Journal Non-Newtonian Fluid Mechanics, Vol. 271, 104144.

Voller V.R., Prakash C. (1987). A Fixed Grid Numerical Modelling Methodology for Convection-Diffusion Mushy Region Phase-Change Problems, International Journal Heat Mass Transfer, Vol. 30(8), pp. 1709–1719.

Wilkinson W.L. (1960). Non-Newtonian fluids. Fluid Mechanics, Mixing and Heat Transfer, London: Pergamon Press.

Zhao J., Zhao W.Q., Chi S.L., Zhu Y.W., Don H. (2020). Quantitative Effects of Different Factors on the Thermal Characteristics of Waxy Crude Oil Pipeline During its Shutdown. Case Studies Thermal Engineering, Vol. 19, 100615

Zhao Y. (2020). Effect of Pipe Diameter on Heat Transfer Characteristics of Waxy Crude Oil Pipeline During Shutdown. Case Studies Thermal Engineering, Vol. 19, 100628.

Zhapbasbayev U.K., Ramazanova G.I., Bossinov D.Zh., Kenzhaliyev B.K. (2021). Flow and Heat Exchange Calculation of Waxy Oil in the Industrial Pipeline. Case Studies Thermal Engineering, Vol. 26, 101007.